Onset of Driven Collisionless Reconnection in Magnetized Pair Plasmas

C. Granier[1], D. Grošelj[1], L. Comisso[2,3], and F. Bacchini[1,4]

[1]*Centre for mathematical Plasma Astrophysics, Department of Mathematics, KU Leuven, Belgium*

[2]*Department of Physics, Columbia University, New York, NY, USA*

[3]*Department of Astronomy, Columbia University, New York, NY, USA*

[4]*Royal Belgian Institute for Space Aeronomy, Belgium*

Abstract

We present 2D particle-in-cell simulations of current-sheet formation, disruption, and nonlinear merging in a strongly magnetized electron–positron plasma. By driving two force-free flux tubes of radius R together at speed $v_{\rm push}$, we observe an exponential collapse. Reconnection onset occurs when the half-thickness reaches $a \simeq d_e$, after

$$t_{\rm onset} \simeq \frac{R}{v_A + v_{\rm push}} \left[1 + \ln \frac{R\, v_A/(v_A + v_{\rm push})}{d_e}\right].$$

Plasmoid chains emerge only for sheet aspect ratios $A = l/a \gtrsim 30$ (where $l$is the sheet length and a a its thickness). In the subsequent merging phase lasting $\Delta t_{\rm merg} \sim 2R/c$, roughly 30% of the reconnecting magnetic energy is dissipated at a normalized rate close to ~ 0.1, largely independent of drive speed or magnetization. These quantitative scalings provide benchmarks for flare models in compact-object magnetospheres.

Introduction Magnetic reconnection, which explains how solar flares release energy [1], is also used to account for bright flares in pulsar wind nebulae [2] and sudden bursts around neutron stars and black holes [3]. In these extreme environments, reconnection happens so fast that it reaches nearly the speed of light [4]. Traditional kinetic studies often begin from preformed Harris sheets or coalescing islands, thereby missing the self-consistent formation of the reconnecting layer. Here, we drive two force-free flux tubes together in a controlled 2D geometry to capture the full lifecycle of the sheet: from formation and kinetic tearing to plasmoid onset and final tubular merger.

Methodology & Evolution Phases We employ the Tristan-MP v2 PIC code in 2D, initializing two Lundquist-type force-free flux tubes [5, 6] of radius R in a cold pair plasma ($\sigma_0 = B_0^2/4\pi n_0 m_e c^2$ from 25 to 800). The tubes are separated by $2R$ in a $4R \times 4R$ domain resolved at $\Delta x = d_e/5$, with $R/d_e \in [50, 1600]$. A uniform inflow $v_{\rm push}$ (so $t_{\rm drive} = R/v_{\rm push}$) is imposed via $\mathbf{E} = -\mathbf{v}_{\rm push} \times \mathbf{B}/c$. We identify three principal phases:

- *Phase I – Sheet Formation:* The current sheet forms, while small-amplitude tearing modes ($k_x d_e \lesssim 1$) grow linearly.

- *Phase II – Plasmoid Formation:* The sheet collapses and nonlinear tearing leads to a chain of plasmoids when $A = \ell/a \gtrsim 30$. The normalized reconnection rates are around 0.002 and 0.02.
- *Phase III – Merging:* Flux tubes coalesce rapidly over $\Delta t_{\rm merg} \sim 2R/c$, with a normalized reconnection rate close to 0.1.

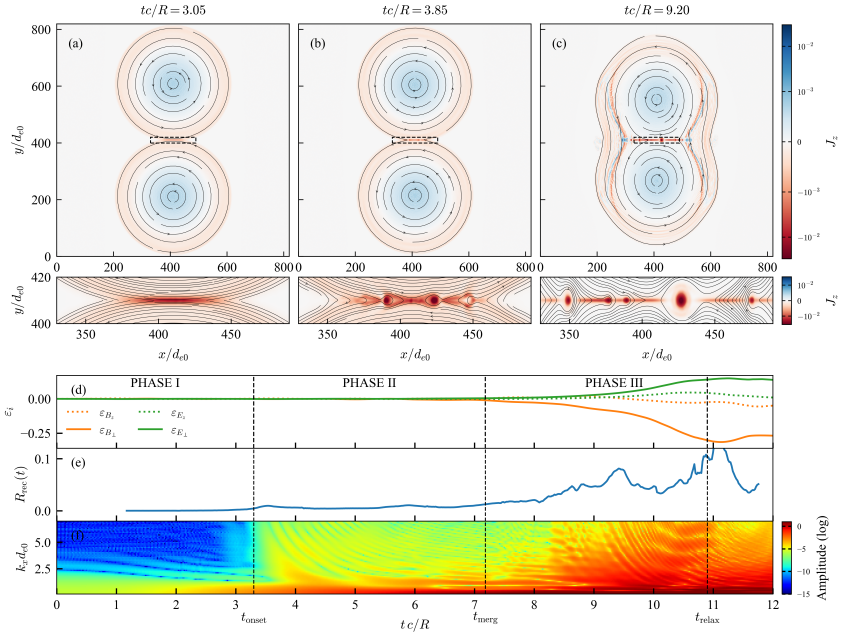

Figure 1: (a)–(c): Contours of out-of-plane current density J_z (color scale) and magnetic field lines (black) during the evolution of the flux tubes. The dashed black boxes mark the regions shown in the zoomed-in view below. (d): Temporal evolution of the energy components, $\varepsilon_i = (E_i(t) - E_i(0))/E_{B_\perp}(0)$. (e): Time evolution of the normalized reconnection rate. (f): k_x-spectra of the magnetic flux function averaged inside the current sheet (over $10d_{e0}$ along y). The color-coded intensity represents the logarithmic amplitude of the wavenumbers. Key time thresholds ($t_{\rm onset}$, $t_{\rm merg}$ and $t_{\rm relax}$) are indicated by vertical dashed lines. This simulation was run with $v_{\rm push} = 0.05c$ ($t_{\rm drive} = 20R/c$), $\sigma_0 = 50$ ($\sigma_{\rm in} = 8$), and $R/d_{e0} = 205$.

Linear Tearing-Mode Growth In our simulations, during Phase I the modes satisfying $k_x d_e \lesssim 1$ exhibit a linear growth rate. Figure 2 plots the logarithmic amplitude of several Fourier modes versus time, confirming that the linear stage ends precisely when the sheet thickness approaches the critical scale a_K.

Onset of Reconnection We derive the onset time by matching the linear thinning and exponential collapse regimes. For $t < t_K$, under the converging inflow $v_{\rm push}$, the two Lundquist tubes of radius R develop a sheet whose half-width $a(t)$ follows first a kinematic thinning (frozen-in drive), $a(t) = R - v_{\rm push}\, t$ with t_k defined as the moment when pinch acceleration $\sim (v_A^2)/a$ becomes comparable to the imposed inflow. Beyond $t > t_K$, the self-pinch ($\mathbf{J} \times \mathbf{B}$ Lorentz force) drives the thinning and yields $da/dt = -a/\tau$ with $\tau = a_K/v_A$, so $a(t - t_K) = a_K\, e^{-(t-t_K)/\tau}$. We equate the external driving time $t_K = (R - a_K)/v_{\rm push}$ with the Alfvén time $t_A = a_K/v_A$ This

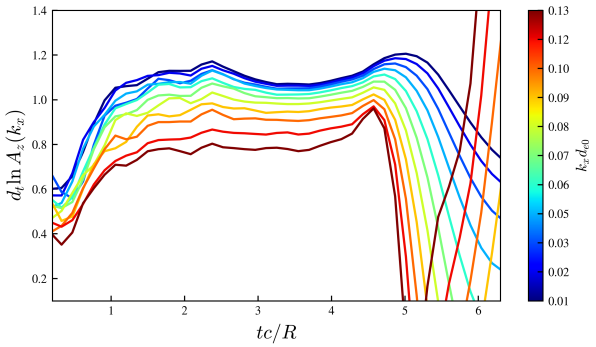

Figure 2: Evolution of tearing-mode amplitudes (log scale) for modes $k_x d_e = 0.5, 0.8, 1.0$ during Phase I. The transition to nonlinear growth coincides with the onset time $t_{\rm onset}$.

yields $t_K \simeq R/v_A + v_{\rm push}$, and $a_K \simeq R v_A/v_A + v_{\rm push}$. Setting $a(t_{\rm onset}) \simeq d_e$ gives

$$t_{\rm onset} \simeq \frac{R}{v_A + v_{\rm push}} \left[1 + \ln \frac{a_K}{d_e}\right]. \tag{1}$$

Figure 3 shows excellent agreement between this prediction and simulation results across a broad range of R/d_e, $v_{\rm push}$, and σ_{in}. The weak dependence on σ_{in} arises because $v_A \simeq c$ when $\sigma_{in} \gg 1$.

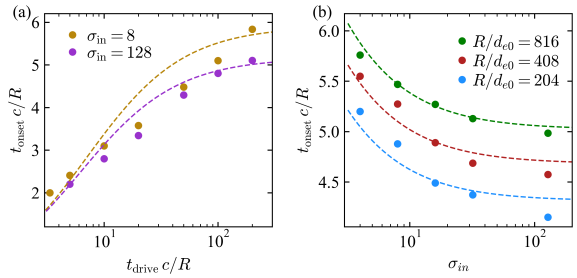

Figure 3: Normalized onset time $t_{\rm onset} c/R$ vs. driving timescale $t_{\rm drive} c/R$ for two magnetizations ($\sigma_{\rm in} = 8, 128$). Symbols: simulation; lines: theoretical prediction.

Reconnection Rate & Dissipation We measure the instantaneous reconnection rate via

$$R_{\rm rec}(t) = \frac{1}{v_A B_{x\rm up}} \frac{d}{dt} \left[\max(A_z) - \min(A_z)\right], \tag{2}$$

where A_z is the out-of-plane component of magnetic vector potential in the midplane between the two tubes (i.e., along the current sheet), and $B_{x\rm up}$ and v_A are the upstream reconnecting field and Alfvén speed (based on $B_{x\rm up}$). Equation (2) measures how fast magnetic flux is transferred across the separatrix.

During rapid merging, the rate saturates near $R_{\rm rec} \sim 0.075$, and the energy-based rate

$$\mathscr{R}_{\rm diss} = \frac{R}{c\,E_{B_\perp}(0)} \frac{d\left[-E_{B_\perp}(t)\right]}{dt} \approx 2\,R_{\rm rec}, \qquad (3)$$

which is the normalized rate of in-plane magnetic energy loss (the factor 2 comes from Poynting inflows on both sides feeding the X-point).

Figure 4 shows $R_{\rm rec} \to 0.1$ in Phase III, independent of drive. The merging duration $\Delta t_{\rm merg} \approx 2R/c$ yields $\langle \mathscr{R}_{\rm diss} \rangle \approx 0.19$.

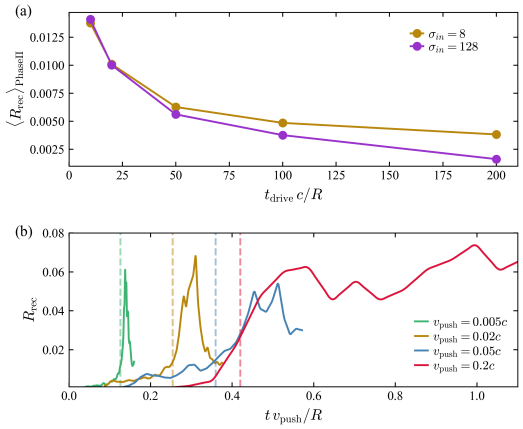

Figure 4: Reconnection rate $R_{\rm rec}(t)$ for various push velocities $v_{\rm push}/c$. The dashed line marks the beginning of Phase III.

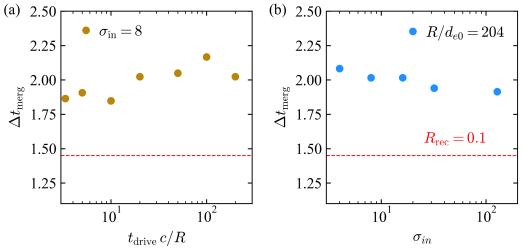

Figure 5: (a) Normalized merging duration $\Delta t_{\rm merg} c/R$ versus driving timescale for $\sigma_{\rm in} = 8$ and $R/d_{e0} = 204$. (b) $\Delta t_{\rm merg}$ versus in-plane magnetization for $t_{\rm drive} c/R = 50$. Start/end defined at 1%/30% energy dissipated.

Conclusions Our 2D PIC simulations of driven collisionless reconnection in strongly magnetized pair show that the onset time follows a simple analytic scaling $\propto R/(c + v_{\rm push})[1 + \ln(Rc/d_e)]$, plasmoids require sheet aspect ratios $\gtrsim 30$, and the merging phase dissipates $\sim 30\%$ of reconnecting energy at a universal rate close to ~ 0.1 (see arXiv [6] for full details).

References

[1] Parker, E. N. 1957, *J. Geophys. Res.*, 62, 509.

[2] Uzdensky, D. A., Cerutti, B., & Begelman, M. C. 2011, *ApJL*, 737, L40.

[3] Thompson, C. 1994, *MNRAS*, 270, 480.

[4] Sironi, L., Uzdensky, D. A., & Giannios, D. 2025, *ARA&A*, 63, doi:10.1146/annurev-astro-020325-115713.

[5] Lyutikov, M., Sironi, L., Komissarov, S. S., & Porth, O. 2017, *J. Plasma Phys.*, 83, 635830602, doi:10.1017/S002237781700071X.

[6] Granier, C., Grošelj, D., Comisso, L., & Bacchini, F. 2025, ApJ, submitted; arXiv:2506.06059.